Laser and Particle Beams (2016), *34*, 539–544.

doi:10.1017/S0263034616000422

Thermodynamic properties of thermonuclear fuel in inertial confinement fusion

V. BRANDON,[1] B. CANAUD,[1] M. TEMPORAL,[2] AND R. RAMIS[3]

[1]CEA, DIF, F-91297 Arpajon, France
[2]Centre de Mathématiques et de Leurs Applications, ENS Cachan and CNRS, UniverSud, 61 Avenue du Président Wilson, F-94235 Cachan Cedex, France
[3]ETSIA, Universidad Politécnica de Madrid, 28040 Madrid, Spain

(RECEIVED 4 May 2016; ACCEPTED 20 June 2016)

Abstract

Hot-spot path in the thermodynamic space $(\rho R, T_i)_{hs}$ is investigated for direct-drive scaled-target family covering a huge interval of kinetic energy on both sides of kinetic threshold for ignition. Different peak implosion velocities and two initial aspect ratios have been considered. It is shown that hot spot follows almost the same path during deceleration up to stagnation whatever the target is. As attended, after stagnation, a clear distinction is done between non-, marginally-, or fully igniting targets. For the last, ionic temperature can reach very high values when the thermonuclear energy becomes very high.

Keywords: Direct drive fusion; Hot-spot; Hydrodynamics calculations; Inertial confinement fusion

Hydrodynamics conditions of the central part of an imploding spherical shell near the stagnation are essential to initiating thermonuclear fusion reactions in the context of inertial confinement fusion (ICF) (Lindl, 1995). Thus, the path to create and sustain thermonuclear fusion blast wave is carefully chosen and determines the total energy gain finally delivered.

In laser-produced ICF (Lindl, 1995), two main ways are considered to realize laser fusion: the indirect drive and the direct drive. The former uses a gold hohlraum to convert laser in X-rays bath that drives the implosion while the later enlightens the spherical pellet directly with well-adapted laser beams. The implosion can be divided into three main parts that are the acceleration stage, the deceleration, and the stagnation. In the first part, drivers accelerate the spherical pellet up to the desired peak implosion velocity. This last is usually defined as the peak average kinetic energy of the remaining shell. When the velocity achieves its maximum value, the deceleration phase begins until the velocity vanishes. It corresponds to stagnation. Whilst the drive is essential for the acceleration stage, deceleration is similar to a free fall path until stagnation. Usually, the implosion is considered isentropic; that means that a Kidder's law-like external pressure is used to accelerate the target. As ideal isentropic compression is not easily achievable with laser, it is currently admitted that a first shock is launched in order to place the fuel in a desired adiabat (defined as the ratio of the shell pressure over the Fermi's pressure). The implosion is done by trying to keep as constant as possible this adiabat. This thermodynamic state is imprinted by the acceleration stage and when deceleration starts, the fuel is in a state that depends on the desired path-to-fusion that designers have chosen.

However, whatever the path-to-fusion chosen, the quest of high gain in thermonuclear fusion is always driven by a global parameter that is the kinetic threshold that depends on adiabat, implosion velocity (Basko, 1995; Piriz, 1996; Levedhal & Lindl, 1997; Basko & Johner, 1998; Lobatchev & Betti, 2000; Herrmann *et al.*, 2001a,b; Kemp *et al.*, 2001; Betti *et al.*, 2002; Canaud *et al.*, 2004; Canaud & Garaude, 2005; Canaud *et al.*, 2007; Cheng *et al.*, 2013) and initial aspect ratio (Brandon *et al.*, 2013a, 2014; Demchenko *et al.*, 2015; Bel'kov *et al.*, 2015). As an evidence, point design below the self-ignition threshold will not be suitable to ignite, deliver, and sustain thermonuclear gain. At the opposite, target design above the self-ignition threshold will deliver high gain. Such kinetic threshold can easily be determined (Canaud *et al.*, 2007; Brandon *et al.*, 2014) by one-dimensional hydrodynamics calculations and a mass rescaling (Basko & Johner, 1998) following a Lie group analysis (Murakami & Iida, 2002) in the context of a similitude theory (Falize *et al.* 2009, 2011). However, such mass rescaling keeps constant only implosion velocity, adiabat, densities, and intensities.

Address correspondence and reprint requests to: B. Canaud, CEA, DIF, F-91297 Arpajon, France. E-mail: benoit.canaud@cea.fr

During the deceleration, a part of the fuel is fully degenerate and coupled. Thus, such an aspect has to be taken into account in the characterization of the state of the matter for thermonuclear fusion (Recoules *et al.*, 2009; Caillabet *et al.*, 2011a). The question of knowing the path of an igniting design in the thermodynamic plan defined by the areal density and the ionic temperature is still of concern. Indeed, hot-spot self-heating conditions (Atzeni & Meyer-ter-Vehn, 2004) coming from a power-balance between the alpha-heating and the thermal and radiative losses represent a curve in such a thermodynamic plan. The representation of hot spot of each design coming from mass rescaling should follow different paths. Among all the designs obtained from the mass rescaling, one corresponds to the kinetic threshold, but another one corresponds to hot-spot self-heating conditions (Hurricane *et al.*, 2014). In addition, in previous works (Brandon *et al.*, 2014), it was shown that another design corresponds to ignition (in the sense of gain one where the gain is the ratio of thermonuclear energy over kinetic energy). Thus, the problem of defining an ignition criteria is still of concern. It requires to identify the path of mass-rescaling designs in the thermonuclear plan and to address the modification of paths when different kinetic thresholds are crossed.

This work addresses the state of the fuel during the deceleration phase of ICF implosion for different mass-rescaled designs on different parts of thresholds (kinetic, gain one, or others). It is organized as follows: in Section 1, the target design and fuel characteristics are described during the deceleration phase. Then Section 2 addresses the mass rescaling technique and the path of each design in the thermodynamic plan defined by the areal density and the average ionic temperature. Each path is the time evolution of both previous quantities during the deceleration.

1. TARGET DESIGN AND HOT-SPOT CHARACTERIZATION DURING DECELERATION

In this work, we consider a target design for which the implosion has been previously optimized (Brandon *et al.*, 2013a, 2014) and defined by its initial aspect ratio: $A = R_{\text{inner}}/(R_{\text{outer}} - R_{\text{inner}}) = 3$. It is a cryogenic spherical layer of deuterium and tritium (DT) at solid density ($\rho = 250\ \text{kg/m}^3$) surrounded by a plastic (CH) ablator and enclosing a DT gas ($\rho = 0.3\ \text{kg/m}^3$). The capsule dimensions and laser pulse are described in Figure 1. This pellet is irradiated by a laser pulse temporally shaped in order to achieve a peak implosion velocity of 300 km/s. Optimization and characterization of the implosion are described in (Brandon *et al.*, 2013a, 2014). This target is marginally igniting that means the thermonuclear energy delivered at stagnation is above the alpha-heating design, corresponding to an alpha-heating produced-energy of the order of the kinetic energy (Herrmann *et al.*, 2001b), and below the self-ignition design, defined as a thermonuclear energy of the order of the absorbed-laser energy (Brandon *et al.*, 2014). This design is one of target set considered for shock ignition on laser MégaJoule (LMJ) (Canaud & Temporal, 2010; Canaud *et al.*, 2012; Brandon *et al.*, 2013b).

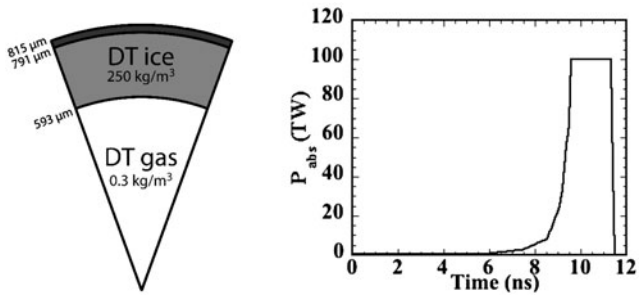

Fig. 1. Target design and laser pulse.

The deceleration phase begins when the shell average-velocity peaks at 300 km/s at the time 11.59 ns, about 140 ps after the laser extinction. During the following 300 ps, the shell velocity vanishes when appears the stagnation. Then shell rebounds. During this phase, the shell density is more and more compressed up to more than $10^6\ \text{kg/m}^3$, while the central ion temperature increases up to 10 keV and the coldest high-density external shell stays about 6–20 eV (see Fig. 2).

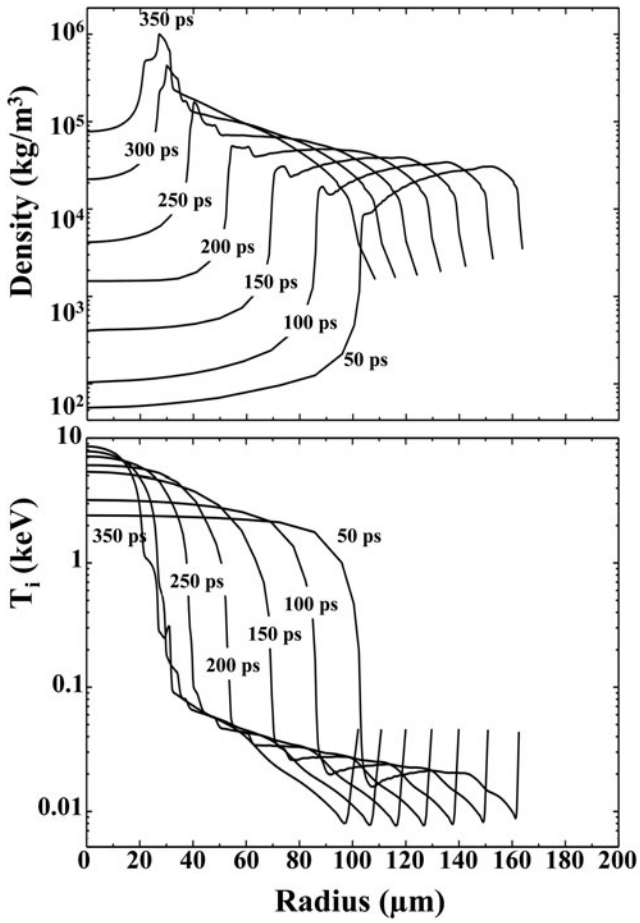

Fig. 2. Density and ionic temperature profiles at selected times during the deceleration.

https://doi.org/10.1017/S0263034616000422 Published online by Cambridge University Press

In a more detailed analysis of the late deceleration-time, very close to the stagnation, it is found that a peak density of $1.2 \times 10^6\,\mathrm{kg/m^3}$ is achieved with an ionic temperature of 330 eV, about 330 ps after the peak velocity.

It is worth noting that, at such density, inter-particle (ions) distance is much smaller than atomic Bohr radius $a_0 \simeq 52.9$ pm. The Wigner–Seitz cell size, $R_{\mathrm{WS}} = [(4/3)\pi n_i]^{-3}$ can give an estimate of average inter-ion distance. Its minimum value varies in time from $R_{\mathrm{WS}} \simeq 30$ pm to less than $a_0/5 \simeq 10$ pm, when the maximum density evolves from 30×10^3 up to $10^6\,\mathrm{kg/m^3}$, respectively.

Everywhere in the dense and compressed shell, electrons are degenerated with a Fermi temperature given by: $T_{\mathrm{F}}^{\mathrm{e}} = (\hbar^2/2k_{\mathrm{B}}m_{\mathrm{e}})\,((6\pi^2/(2s+1))n_{\mathrm{e}}[\mathrm{m}^{-3}])^{2/3}$, where $s = 1/2$ is the electronic spin. Thus, $T_{\mathrm{F}}^{\mathrm{e}}[\mathrm{eV}] \simeq 0.14(\rho[\mathrm{kg \cdot m^{-3}}])^{2/3}$ and $\Theta_{\mathrm{F}}^{\mathrm{e}} = T_{\mathrm{e}}/T_{\mathrm{F}}^{\mathrm{e}}$ evolve in the dense shell between 0.09 and 0.25.

In addition, the electronic and ionic plasma-coupling parameter $\Gamma_\alpha = e^2/(12\pi\epsilon_0 R_{\mathrm{WS}} k_{\mathrm{B}} T_\alpha)$ with $\alpha = \{e, D, T\}$ evolve between 0.6 and 1.6 over the shell and during the whole deceleration.

We compare also the De Broglie length $\lambda_\alpha = \hbar\sqrt{2\pi/(m_\alpha k_{\mathrm{B}} T_\alpha)}$ for $\alpha = \{e, D, T\}$, to the Wigner–Seitz radius in the dense part of the shell and we found that $R_{\mathrm{WS}} \simeq 0.2\lambda_e \simeq 25\lambda_D \simeq 30\lambda_T$. Finally, by regarding all these quantities, we can conclude that quantum effects and strong coupling exist for electrons, while ions are only strongly coupled but not degenerated.

2. ICF-PARAMETRIZATION

In this section, we consider different peak velocities and initial aspect ratios ($A = 3$ and 5). First, we focus on $A = 3 - v = 300\,\mathrm{km/s}$ target (Brandon *et al.*, 2013a, 2014).

For each design of the edge of the cloud of optimization, hydrodynamic scaling is performed and self-ignition threshold is determined [for more details see Figs 3 and 13 of Brandon *et al.* (2014)].

2.1 Mass-rescaling

The hydrodynamics scaling is achieved by multiplying times and lengths by a factor s, power by s^2, and energies and masses by s^3. This hydrodynamics scaling defines a "homothetic target family" (Canaud *et al.*, 2004; Canaud & Garaude, 2005; Canaud *et al.*, 2007; Brandon *et al.*, 2013a) in the context of ICF parameterized by invariants, that is, peak implosion velocities, densities, and intensities. Such an approach is used to estimate the scaling of minimum kinetic energy for ignition (Cheng *et al.*, 2013; Brandon *et al.*, 2014).

Then, one-dimensional calculations are done for each target design defined by the scaling factor s and thermonuclear energy is given in Figure 3 as a function of the peak kinetic energy. The last is varying due to the mass variation, while peak implosion velocity being the same at 300 km/s. The target gain one, that can be defined as the alpha heating

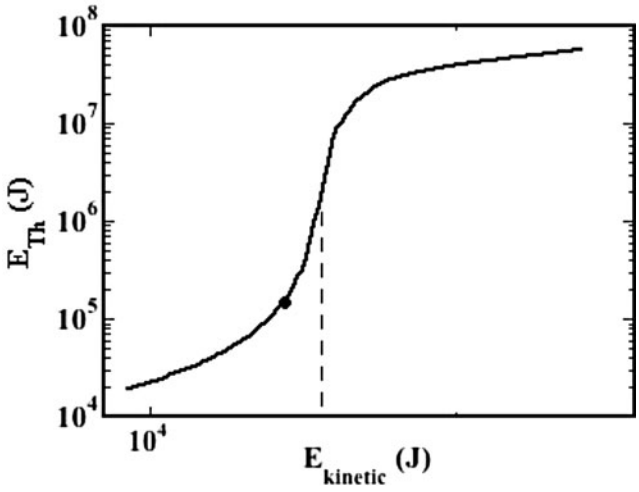

Fig. 3. Thermonuclear energy versus the peak kinetic energy for different scaling. The dot represents the scaling $s = 1$.

equivalent to shell kinetic energy, is achieved here at a kinetic energy of approximately 5 kJ. For this target, hydrodynamic efficiency is constant at 6%. Thus, absorbed energy is approximately 80 kJ.

The kinetic energy threshold represents the transition between two distinct regimes (asymptotes in the figure) corresponding to the hot-spot formation and the shell burn-out. The black dot corresponds to the initial target design presented in Figure 1. It is a marginally igniting target (target gain > 1 and thermonuclear gain < 1). In the previous papers (Brandon *et al.*, 2013a, 2014), two distinct thresholds were considered for this scaling: the first one is corresponding to the target gain one and the second one to the maximum of the gradient of the curve. Each threshold does not correspond to the same design.

Deceleration of each design represents a path in the thermodynamic plan (areal density vs. ionic temperature) for the hot spot that is shown in Figure 4. On the same plot,

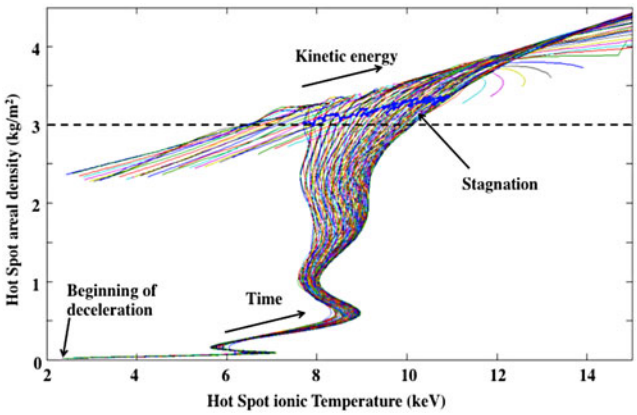

Fig. 4. Hot-spot path in the thermodynamic plan. Each curve addresses a specific Direct Drive design in the scaling curve. Blue dots represent the stagnation. Dashed line corresponds to ignition condition $\rho r \sim 3\,\mathrm{kg/m^2}$.

https://doi.org/10.1017/S0263034616000422 Published online by Cambridge University Press

areal densities and temperatures are given at the stagnation time (dots). The upper limit of the areal density versus the temperature is bounded by homothetic transformation and increases with s.

It is worth noting that all the curves follow similar paths during the deceleration up to stagnation. The classical ignition conditions ($\rho R > 3$ kg/m^2 and T_i>6 keV (Atzeni & Meyer-ter-Vehn, 2004) are met whatever target is in the homothetic family. In addition, temperatures reach very large values above 8 keV. Indeed, during this violent collapse, strong shock waves travel through and focus at the target center increasing the ionic hot-spot temperature. However, hot-spot temperature results as an energy balance between alpha redeposition and thermal and radiative losses. Thus, while in principle, temperatures scale as the energy (i.e., s^3), and areal density as space (i.e., s), the ignition brakes the scaling variations. It is more or less precluded in the ignition criterion (Atzeni & Meyer-ter-Vehn, 2004). Indeed, looking at Figure 4, a difference exists in the curves of non- or marginally igniting targets and burning targets. For non-igniting target, nuclear fusion reactions take place in the hot spot, increasing perturbatively the pressure at stagnation. Nevertheless, the kinetic energy still present in the shell is not strong enough to ignite the shell. For the marginally igniting targets (in the cliff of Fig. 3), alpha redeposition increases the hot-spot pressure significantly of the same order than mechanical (PdV) work. At stagnation, some kinetic energy is still available in the shell and, thus, the hot-spot temperature starts to increase after stagnation. For targets with kinetic energies higher than the self-ignition threshold (well above the cliff in Fig. 3), ignition and alpha redeposition become dominant and stagnation occurs, while a significant amount of kinetic energy is still available in the shell. This kinetic margin (seen as the shell kinetic of an implosion without thermonuclear fusion is taken at stagnation time of implosion with fusion) results in an increase of the hot-spot temperature that amplifies thermonuclear reactions and burn. This leads to very high ionic temperatures (above 100 keV).

2.2 Effect of peak implosion velocity

The next step is to know if the implosion velocity could be a relevant parameter that could modify the hot-spot path.

Using the data set previously obtained from dedicated implosion design studies (Brandon *et al.*, 2013a, 2014) for the $A = 3$ capsules, different implosion velocities are considered. Hydrodynamic scalings were done. Hot-spot path in the thermodynamic plane is thus estimated for each peak implosion velocity and given in Figure 5. It is worth noting that implosion velocity has no significant effect on the hot-spot path of each target scaling during the deceleration.

2.3 Effect of initial aspect ratio

An additional key aspect is the initial aspect ratio A (Brandon *et al.*, 2013a, 2014; Demchenko *et al.*, 2015). In this section, we analyze a different capsule characterized by an aspect ratio $A = 5$. Optimization was randomly performed and described in (Brandon *et al.*, 2013a, 2014). We analyze the deceleration phase of the implosion as is done in the previous section.

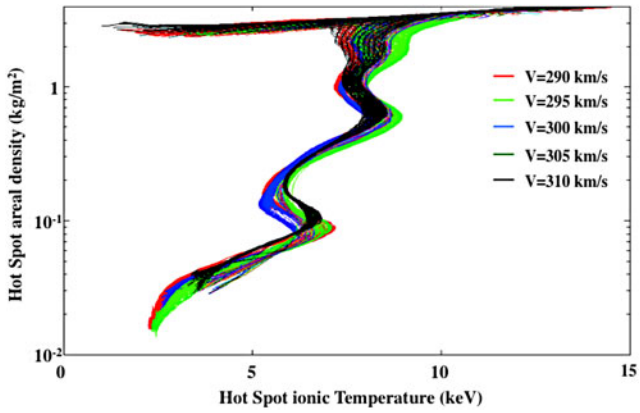

Fig. 5. Hot-spot path in the thermodynamic plan for different scaling and for different peak implosion velocities.

Results are summarized in Figure 6 for different implosion velocities. Surprisingly, the curves show the same trend than for $A = 3$ even if they are not exactly the same. The hot spot seems to follow a path during deceleration that is not significantly dependent of the initial target specifications. This assertion is under the assumption that the implosion has been optimized previously in the same way.

Nevertheless, whatever the ICF parameters are (we mean implosion velocity and initial aspect ratio), hot spot during the deceleration describes a path in the (T_i, ρr) plane that is always inside a pattern. This specificity is a mix between implosion and specifically optimizing shock timing, history, and numerical models [thermal conductivities (Recoules *et al.*, 2009), DT equation of states (Caillabet *et al.*, 2011b), etc.].

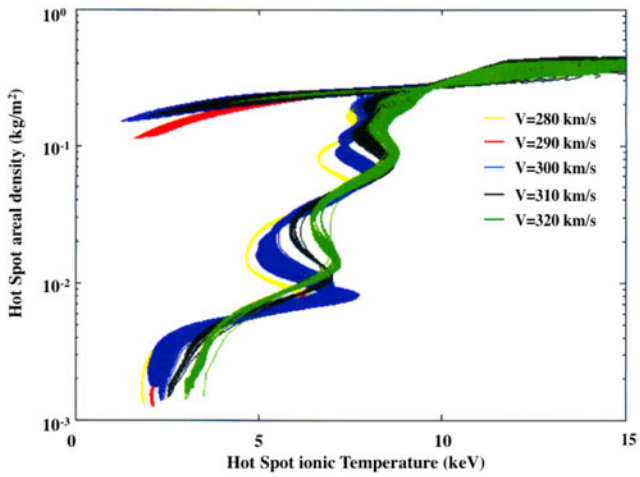

Fig. 6. Hot-spot path in the thermodynamic plan for different scaling, for different peak implosion velocities and an initial aspect ratio $A = 5$.

https://doi.org/10.1017/S0263034616000422 Published online by Cambridge University Press

Experimental measurements of ionic temperatures at neutron emission times, as usually done on OMEGA (Glebov *et al.*, 2004) or NIF (Glebov *et al.*, 2010, 2012; Hurricane *et al.*, 2014) could be used for testing models employed in our codes. Nevertheless, DT stratification in the hot spot (Amendt *et al.*, 2010; Amendt *et al.*, 2011; Bellei *et al.*, 2013) could lead to ion thermal decoupling (Inglebert *et al.*, 2014; Rinderknecht *et al.*, 2015) and could introduce mistake or misunderstanding in the hot-spot thermodynamics.

3. CONCLUSIONS

In this work, we present a numerical analysis of hot-spot path in the thermodynamical plane (T_i, ρR) of direct-drive imploding targets. The parameters characterizing this path are followed in time from the beginning of deceleration to after stagnation.

Different parametric variations have been done.

First a hydrodynamic scaling is performed for each implosion velocity. Different implosion velocities are considered and also two initial aspect ratios.

All these parameter variations show that hot spot of an ICF target follows almost the same path during the whole deceleration. After stagnation, a difference is seen between non-igniting, marginally, or fully igniting targets.

REFERENCES

Amendt, P., Landen, O.L., Robey, H.F., Li, C.K. & Petrasso, R.D. (2010). Plasma barodiffusion in inertial-confinement-fusion implosions: application to observed yield anomalies in thermonuclear fuel mixtures. *Phys. Rev. Lett.* **105**, 115005.

Amendt, P., Wilks, S.C., Bellei, C., Li, C.K. & Petrasso, R.D. (2011). The potential role of electric fields and plasma barodiffusion on the inertial confinement fusion database. *Phys. Plasmas* **18**, 056308.

Atzeni, S. & Meyer-ter-Vehn, J. (2004). *The physics of inertial fusion*. Oxford: Clarendon Press-Oxford.

Basko, M. (1995). On the scaling of the energy gain of ICF targets. *Nucl. Fusion* **35**, 87.

Basko, M. & Johner, J. (1998). Ignition energy scaling of inertial confinement fusion targets. *Nucl. Fusion* **38**, 1779.

Bel'kov, S.A., Bondarenko, S.V., Vergunova, G.A., Garanin, S.G., Gus'kov, S.Y., Demchenko, N.N., Doskoch, I.Y., Kuchugov, P.A., Zmitrenko, N.V., Rozanov, V.B., Stepanov, R.V. & Yakhin, R.A. (2015). Thermonuclear targets for direct-drive ignition by a Megajoule laser pulse. *J. Exp. Theor. Phys.* **121**, 686–698.

Bellei, C., Amendt, P.A., Wilks, S.C., Haines, M.G., Casey, D.T., Li, C.K., Petrasso, R. & Welch, D.R. (2013). Species separation in inertial confinement fusion fuels. *Phys. Plasmas* **20**, 012701.

Betti, R., Anderson, K., Goncharov, V.N., McCrory, R.L., Meyerhofer, D.D., Skupsky, S. & Town, R. (2002). Deceleration phase of inertial confinement fusion implosions. *Phys. Plasmas* **9**, 2277.

Brandon, V., Canaud, B., Laffite, S., Temporal, M. & Ramis, R. (2013a). Marginally igniting direct-drive target designs for the laser Megajoule. *Laser Part. Beams* **31**, 141.

Brandon, V., Canaud, B., Laffite, S., Temporal, M. & Ramis, R. (2013b). Systematic analysis of direct-drive baseline designs for shock ignition with the laser Megajoule. *EPJ: Web Conf.* **59**, 03004.

Brandon, V., Canaud, B., Temporal, M. & Ramis, R. (2014). Low initial aspect-ratio direct-drive target designs for shock- or self-ignition in the context of the laser Megajoule. *Nucl. Fusion* **54**, 083016.

Caillabet, L., Canaud, B., Salin, G., Mazevet, S. & Loubeyre, P. (2011a). Change in inertial confinement fusion implosions upon using an ab initio multiphase DT equation of state. *Phys. Rev. Lett.* **107**, 115004.

Caillabet, L., Mazevet, S. & Loubeyre, P. (2011b). Multi-phases equation of state of hydrogen from ab-initio calculations in the range 0.2 to 5 g/CC up to 10 eV. *Phys. Rev. B* **83**, 094101.

Canaud, B., Fortin, X., Garaude, F., Meyer, C., Philippe, F., Temporal, M., Atzeni, S. & Schiavi, A. (2004). High gain direct-drive target design for the laser Megajoule. *Nucl. Fusion* **44**, 1118.

Canaud, B. & Garaude, F. (2005). Optimization of laser-target coupling efficiency for direct drive laser fusion. *Nucl. Fusion* **45**, L43.

Canaud, B., Garaude, F., Clique, C., Lecler, N., Masson, A., Quach, R. & Van der Vliet, J. (2007). High-gain direct-drive laser fusion with indirect drive beam layout of laser Mégajoule. *Nucl. Fusion* **47**, 1652.

Canaud, B. & Temporal, M. (2010). High-gain shock ignition of direct-drive ICF targets for the laser Mégajoule. *New J. Phys.* **12**, 043037.

Canaud, B., Temporal, M. & Laffite, S. (2012). 2D analysis of direct-drive shock-ignited HiPER-like target implosions with the full laser megajoule for the laser Megajoule. *Laser Part. Beams* **30**, 183.

Cheng, B., Kwan, T.J.T., Wang, Y.-M. & Batha, S.H. (2013). Scaling laws for ignition at the National Ignition facility from first principles. *Phys. Rev. E* **88**, 041101.

Demchenko, N.N., Doskoch, I.Y.A., Gus'kov, S.Y., Kuchugov, P.A., Rozanov, V.B., Stepanov, R.V., Vergunova, G.A., Yakhin, R.A. & Zmitrenko, N.V. (2015). Irradiation asymmetry effects on the direct drive targets compression for the megajoule laser facility. *Laser Part. Beams* **33**, 655.

Falize, E., Bouquet, S. & Michaut, C. (2009). Scaling laws for radiating fluids: the pillar of laboratory astrophysics. *Astrophys. Space Sci.* **322**, 107.

Falize, E., Michaut, C. & Bouquet, S. (2011). Similarity properties and scaling laws of radiation hydrodynamic flows in laboratory astrophysics. *Astrophys. J.* **730**, 96.

Glebov, V.Y., Forrest, C., Knauer, J.P., Pruyne, A., Romanofsky, M., Sangster, T.C., Shoup III., M.J., Stoeckl, C., Caggiano, J.A., Carman, M.L., Clancy, T.J., Hatarik, R., McNaney, J. & Zaitseva, N.P. (2012). Testing a new NIF neutron time-of-flight detector with a bibenzyl scintillator on OMEGA. *Rev. Sci. Instrum.* **83**, 10D309.

Glebov, V.Yu, Sangster, T.C., Stoeckl, C., Knauer, J.P., Theobald, W., Marshall, K.L., Shoup III., M.J., Buczek, T., Cruz, M., Duffy, T., Romanofsky, M., Fox, M., Pruyne, A., Moran, M.J., Lerche, R.A., McNaney, J., Kilkenny, J.D., Eckart, M.J., Schneider, D., Munro, D., Stoeffl, W., Zacharias, R.,

https://doi.org/10.1017/S0263034616000422 Published online by Cambridge University Press

Haslam, J.J., Clancy, T., Yeoman, M., Warwas, D., Horsfield, C.J., Bourgade, J.-L., Landoas, O., Disdier, L., Chandler, G.A. & Leeper, R.J. (2010). The National Ignition Facility neutron time-of-flight system and its initial performance. *Rev. Sci. Instrum.* **81**, 10D325.

Glebov, V.Yu, Stoeckl, C., Sangster, T.C., Roberts, S., Schmid, G.J., Lerche, R.A. & Moran, M.J. (2004). Prototypes of National Ignition Facility neutron time-of-flight detectors tested on OMEGA. *Rev. Sci. Instrum.* **75**, 3559.

Herrmann, M., Tabak, M. & Lindl, J. (2001a). A generalized scaling law for the ignition energy of inertial confinement fusion capsules. *Nucl. Fusion* **41**, 99.

Herrmann, M., Tabak, M. & Lindl, J. (2001b). Ignition scaling laws and their application to capsule design. *Phys. Plasmas* **8**, 2296.

Hurricane, O.A., Callahan, D.A., Casey, D.T., Celliers, P.M., Cerjan, C., Dewald, E.L., Dittrich, T.R., Doppner, T., Hinkel, D.E., Berzak-Hopkins, L.F., Kline, J.L., Pape, S.L., Ma, T., MacPhee, A.G., Milovich, J.L., Pak, A., Park, H.S., Patel, P.K., Remington, B.A., Salmonson, J.D., Springer, P.T. & Tommasini, R. (2014). Fuel gain exceeding unity in an inertially confined fusion implosion. *Nature* **506**, 343–348.

Inglebert, A., Canaud, B. & Larroche, O. (2014). Species separation and neutron yield modification in inertial-confinement fusion. *Eur. Phys. Lett.* **107**, 65003.

Kemp, A., Meyer-ter-Vehn, J. & Atzeni, S. (2001). Stagnation pressure of imploding shells and ignition energy scaling of inertial confinement fusion targets. *Phys. Rev. Lett.* **86**, 3336.

Levedhal, W. & Lindl, J. (1997). Energy scaling of inertial confinement fusion targets for ignition and high gain. *Nucl. Fusion* **37**, 165.

Lindl, J. (1995). Development of the indirect-drive approach to inertial confinement fusion and the target physics basis for ignition and gain. *Phys. Plasmas* **2**, 3933.

Lobatchev, V. & Betti, R. (2000). Ablative stabilization of the deceleration phase rayleigh-taylor instability. *Phys. Rev. Lett.* **85**, 4522.

Murakami, M. & Iida, S. (2002). Scaling laws for hydrodynamically similar implosions with heat conduction. *Phys. Plasmas* **9**, 2745.

Piriz, A.R. (1996). Scaling Laws for the ignition of deuterium-tritium shell targets. *Fusion Eng. Des.* **32&33**, 561.

Recoules, V., Lambert, F., Decoster, A., Canaud, B. & Clerouin, J. (2009). Ab initio determination of thermal conductivity of dense hydrogen plasmas. *Phys. Rev. Lett.* **102**, 075002.

Rinderknecht, H.G., Rosenberg, M.J., Li, C.K., Hoffman, N.M., Kagan, G., Zylstra, A.B., Sio, H., Frenje, J.A., Gatu Johnson, M., Séguin, F.H., Petrasso, R.D., Amendt, P., Bellei, C., Wilks, S., Delettrez, J., Glebov, V.Y., Stoeckl, C., Sangster, T.C., Meyerhofer, D.D. & Nikroo, A. (2015). Ion thermal decoupling and species separation in shock-driven implosions. *Phys. Rev. Lett.* **114**, 025001.

https://doi.org/10.1017/S0263034616000422 Published online by Cambridge University Press